7 June 1985, Volume 228, Number 4704 SCIENCE

Imaging Spectrometry for Earth Remote Sensing

Alexander F. H. Goetz, Gregg Vane
Jerry E. Solomon, Barrett N. Rock

Summary. Imaging spectrometry, a new technique for the remote sensing of the earth, is now technically feasible from aircraft and spacecraft. The initial results show that remote, direct identification of surface materials on a picture-element basis can be accomplished by proper sampling of absorption features in the reflectance spectrum. The airborne and spaceborne sensors are capable of acquiring images simultaneously in 100 to 200 contiguous spectral bands. The ability to acquire laboratory-like spectra remotely is a major advance in remote sensing capability. Concomitant advances in computer technology for the reduction and storage of such potentially massive data sets are at hand, and new analytic techniques are being developed to extract the full information content of the data. The emphasis on the deterministic approach to multispectral data analysis as opposed to the statistical approaches used in the past should stimulate the development of new digital image-processing methodologies.

Remote sensing of the earth's surface from aircraft and from spacecraft provides information not easily acquired by surface observations. Until recently, the main limitations of remote sensing were that no subsurface information could be acquired and that surface information lacked specificity (*1*). Orbital imaging radar can now provide subsurface data in arid regions (*2*), and recent work in high-spectral-resolution radiometry shows that mineral components in the surface, as well as vegetation stressed by metals in the substrate, can be identified (*3*). In this article we discuss early results of a major advance in remote sensing, imaging spectrometry, which consists of the acquisition of images in many narrow contiguous spectral bands throughout the visible and solar-reflected infrared portions of the spectrum. In addition, we discuss several approaches to the analysis of the resulting hyperspectral image data sets. Hyperspectral refers to the multidimensional character of the spectral data set. In the past, data were acquired in four to seven spectral bands. Imaging spectrometry now makes possible the acquisition of data in hundreds of spectral bands simultaneously. Because of the specificity of the data acquired by imaging spectrometry, many more problems can now be addressed by this remote sensing technique.

The value of the technique lies in its ability to acquire a complete reflectance spectrum for each picture element (pixel) in the image. The reflectance spectrum in the region 0.4 to 2.5 μm can be used to identify a large range of surface cover materials that cannot be identified with broadband, low-resolution imaging systems such as the Landsat scanners (*4*). Figure 1 shows high-spectral-resolution laboratory reflectance spectra for a number of common minerals. The Landsat thematic mapper (TM) is able to acquire only one data point in this wavelength region. Many surface materials, although not all, have diagnostic absorption features that are 20 to 40 nm wide at half the band depth (*5*). Therefore, spectral imaging systems, which acquire data in contiguous 10-nm-wide bands, can produce data with sufficient resolution for the direct identification of those materials with diagnostic spectral features. The Landsat scanners, which have bandwidths between 100 and 200 nm, cannot resolve these spectral features. Some important rock-forming minerals, such as quartz and feldspar, do not have any fundamental or overtone absorption features in the region from 0.4 to 2.5 μm and therefore cannot be detected directly. On the other hand, neither do these minerals mask the absorption features of the important minor minerals in rocks and soils. Similarly, mineral mixtures, and mixtures with vegetation in an individual pixel, can be separated if the components have unique spectral features.

Data Collection

Simultaneous imaging in many contiguous spectral bands requires a new approach to sensor design. Sensors such as the Landsat multispectral scanner (MSS) or TM are optomechanical systems in which discrete detector elements are scanned across the surface of the earth perpendicular to the flight path, and these detectors convert the reflected solar photons from each pixel in the scene into a sensible electronic signal (Fig. 2a). The detector elements are placed behind filters that pass broad portions of the spectrum. The MSS has four such sets of filters and detectors, whereas TM has seven. The primary limitation of this approach is the short residence time of the detector in each instantaneous field of view (IFOV). To achieve adequate signal-to-noise ratio without sacrificing spatial resolution, such a sensor must operate in broad spectral bands of 100 nm or greater or must use optics with unrealistically small ratios of focal length to aperture (*f* numbers).

One approach to increasing the residence time of a detector in each IFOV is

A. F. H. Goetz is a senior research scientist and imaging spectrometer program manager, G. Vane is a member of the technical staff, J. E. Solomon is the supervisor of the imaging analysis systems group, and B. N. Rock is the supervisor of the geobotanical remote sensing group, Jet Propulsion Laboratory, California Institute of Technology, Pasadena 91109.

to use line arrays of detector elements (Fig. 2b). In this configuration there is a dedicated detector element for each cross-track pixel, which increases the residence or integration time to the interval required to move one IFOV along the track. Such an experimental two-spectral channel instrument, called the modular optoelectronic multispectral scanner, has been carried aboard the space shuttle (*6*). A French satellite sensor called SPOT (Systeme Probatoire d'Observation de la Terre) that will use line array detectors will be launched in 1985. It is expected that this system will provide stereoscopic image capability in three spectral bands in the region short of 1.0 μm (*7*).

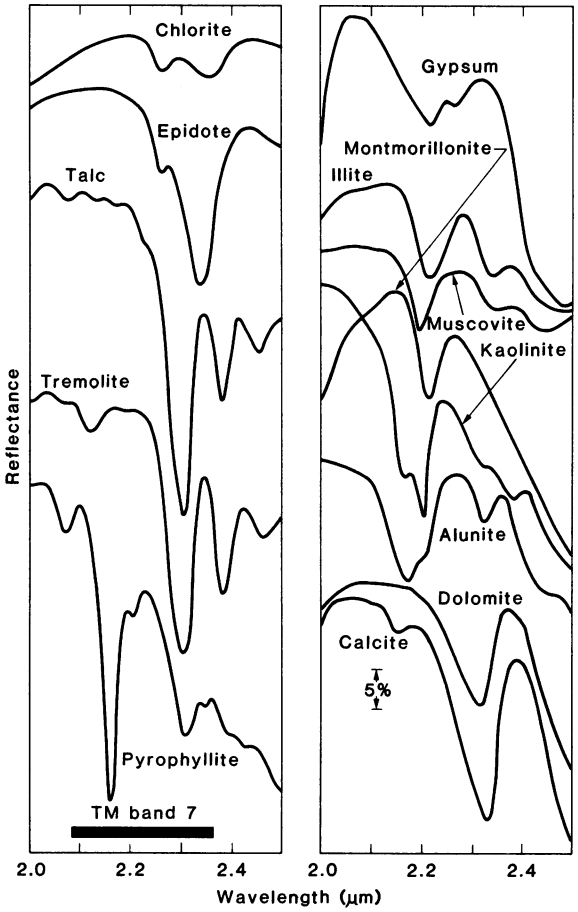

Fig. 1. Selected laboratory spectra of minerals containing overtone vibrational absorption features for Al–OH (2.16 to 2.22 μm), Mg–OH (2.3 to 2.35 μm), and CO_3 (2.3 to 2.35 μm). The band 7 bandwidth of the Landsat thematic mapper is also shown.

There are limitations and trade-offs associated with the use of multiple line arrays, each having its own spectral band-pass filter. If all the arrays are placed in the focal plane of the telescope, then the same ground locations are not imaged simultaneously in each spectral band. If beam splitters are used to facilitate simultaneous data acquisition, the signal is reduced by 50 percent or more for each additional spectral band acquired in a given spectral region. Furthermore, instrument complexity increases substantially if more than six to ten spectral bands are desired.

Two approaches to imaging spectrometry are shown in Fig. 2, c and d. The line array approach (Fig. 2c) is analogous to the scanner approach used for MSS or TM except that light from a pixel is passed into a spectrometer where it is dispersed and focused onto a line array. Thus each pixel is simultaneously sensed in as many spectral bands as there are detector elements in the line array. For high-spatial-resolution imaging (ground IFOV's of 10 to 30 m), this approach is suited only to an airborne sensor which flies slowly enough that the readout time of the detector array is a small fraction of the integration time. Because of the high spacecraft velocities, imaging spectrometers designed for Earth orbit require the use of two-dimensional area arrays of detectors at the focal plane of the spectrometer (Fig. 2d), obviating the need for the optical scanning mechanism. In this situation there is a dedicated column of spectral detector elements for each cross-track pixel in the scene.

The key, then, to imaging spectrometry is the detector array. Line arrays of silicon, sensitive from about 0.35 to 1.1 μm, are available commercially in dimensions up to 5000 elements in length (*8*). Area arrays of up to 800 by 800 elements of silicon were developed for the Galileo Jupiter camera and for the Space Telescope wide field and planetary camera (*9*), and an experimental 1024 by 1024 device has been recently tested (*10*). However, the state of infrared array development is not yet so advanced. Line arrays are available in several materials up to a few hundred detector elements in length. Two of the most attractive materials are mercury cadmium telluride (HgCdTe) and indium antimonide (InSb); InSb line arrays of 512 elements having very high quantum efficiency and detector element-to-element responsivity uniformity have been

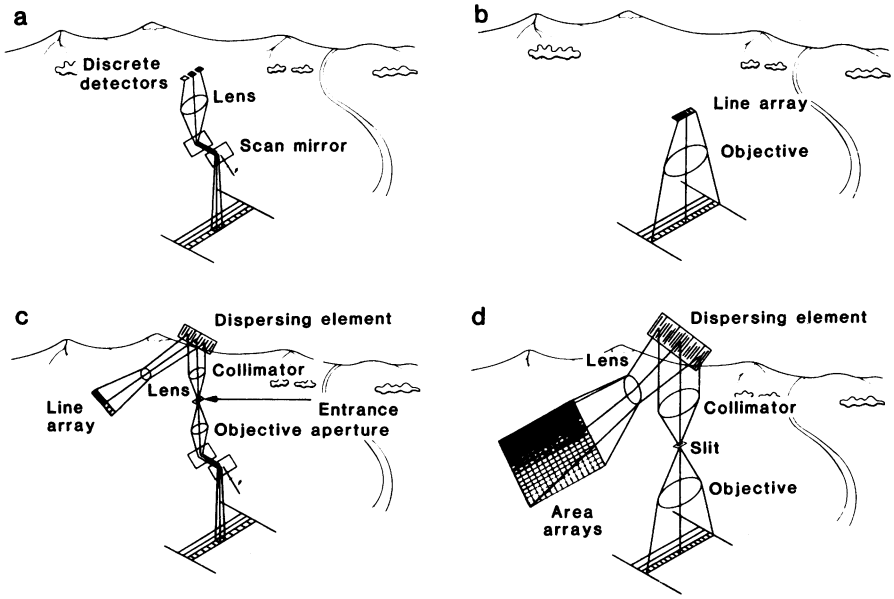

Fig. 2. Four approaches to sensors for multispectral imaging: (a) multispectral imaging with discrete detectors; (b) multispectral imaging with line arrays; (c) imaging spectrometry with line arrays; and (d) imaging spectrometry with area arrays.

developed (*11*). These arrays respond to wavelengths from about 0.7 to 5.2 μm.

For area arrays, 32 by 32 element devices of HgCdTe sandwiched with a silicon charged-couple device multiplexer have been made successfully (*12*), and 64 by 64 element devices, which can be abutted on opposite sides, are under development (*13*). These devices can be mosaicked to form focal plane arrays of 64 by 64*n* elements in dimension, where *n* represents the number of devices in the mosaic. Although development of 64 by 64 element devices is progressing, the 32 by 32 element array represented the state of the art in infrared area arrays 2 years ago, when the first airborne sensor was being tested.

A sensor called the airborne imaging spectrometer (AIS) has been built to test the imaging spectrometer concept with infrared area arrays (*14*). This instrument operates in the mode shown in Fig. 2d. The spectral coverage of the instrument is 1.2 to 2.4 μm, in contiguous bands that are 9.3 nm wide. This sampling interval is sufficient to completely describe absorption features for solids in this wavelength region. Continuous strip images, 32 pixels wide in 128 spectral bands, are acquired from the National Aeronautics and Space Administration (NASA) C-130 aircraft. The 128 spectral bands are acquired by stepping the spectrometer grating through four positions during the time it takes to fly forward one pixel width on the ground. The area array is read out between each grating position, and the data are recorded on the aircraft with a high-density analog tape recorder. The IFOV of AIS is 1.9 milliradians, which produces a ground pixel size of approximately 8 by 8 m from a typical operating altitude of 4200 m. To aid in locating the AIS ground track, a boresighted 35-mm camera acquires black and white, wide-field-of-view photography.

Figure 3 shows an AIS image, acquired over Van Nuys, California, on the first engineering flight of AIS in November 1982. This image covers the area outlined in black lines on the camera photograph. Notable features include a field in the lower portion of the image, a condominium complex in the center, and a school in the upper half of the image. On this test flight, images were acquired in only one grating position, or in 32 contiguous spectral bands in the region from 1.5 to 1.2 μm. A mosaic of the 32 AIS images, each in a different 9.3-nm-wide spectral band and each 32 pixels wide, is shown below the photograph. The most obvious feature in the mosaic is the loss of detail in the 1.4-μm atmospheric water absorption band. However, there is considerable detail visible in the spectral images well inside this band. Details associated with reflectance variations are identified with arrows. For instance, the reflectance of a well-watered courtyard lawn inside the school grounds

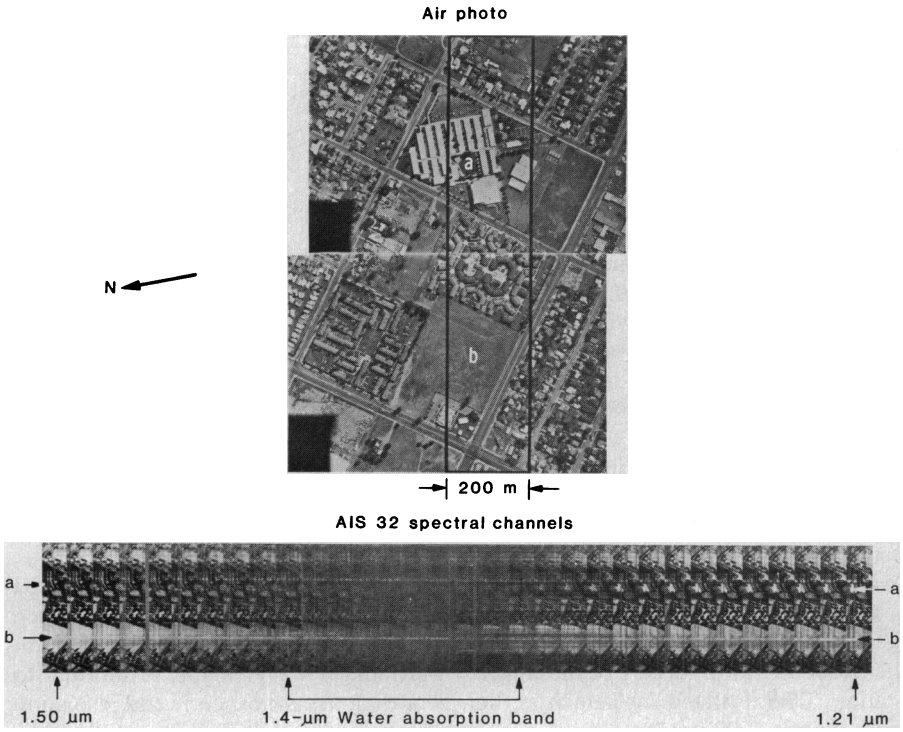

Fig. 3. Air photo of an area in Van Nuys, California, showing a school courtyard (a) and an open field (b). The black traces outline the coverage of the 32-pixel-wide AIS images taken in 32 spectral bands between 1.50 and 1.21 μm. The individual AIS images taken in 9.3-nm-wide, contiguous spectral intervals are shown at the bottom. The spectral reflectance behavior of the well-watered courtyard and the open field are quite different and reflect the irrigation practices.

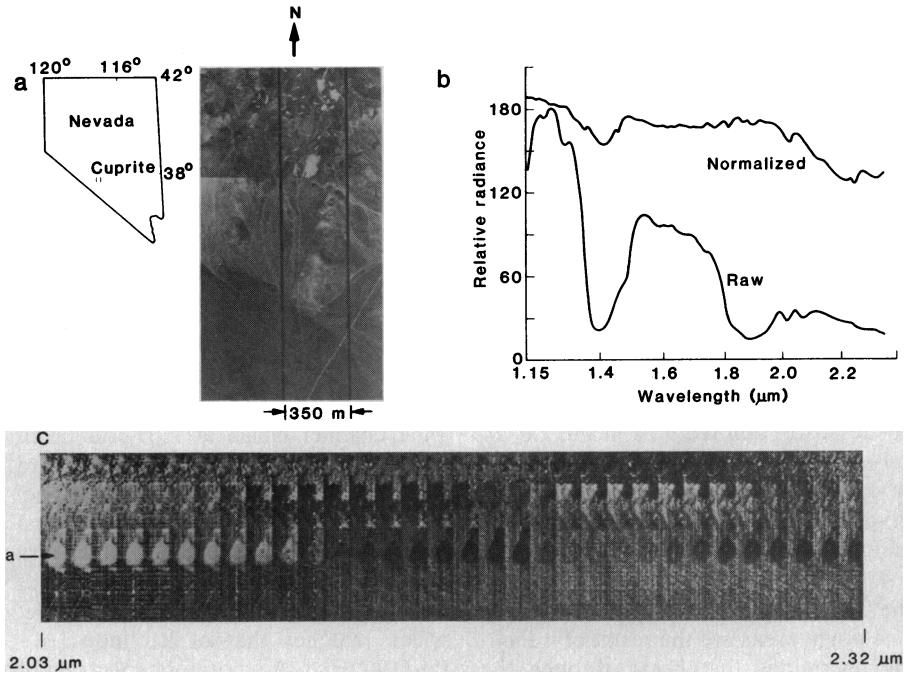

Fig. 4. (a) Air photo of a portion of the Cuprite mining district in Nevada, superimposed with the AIS coverage. (b) Spectra (128 channels) derived from a 5 by 5 pixel area in the AIS image of the Cuprite mining district. The normalized spectrum approximates the ground spectral reflectance. (c) A set of 32 AIS spectral images over Cuprite taken at 9.3-nm intervals between 2.03 and 2.32 μm in which each pixel spectrum has been normalized to produce an equal area under the reflectance curve. The differing reflectance characteristics as a function of wavelength are clearly visible (location a).

(location a) drops significantly beyond 1.4 μm in comparison with the reflectance of the unwatered field (location b).

The AIS instrument was designed primarily as an engineering test bed for detector development, but it has been used successfully for data acquisition in support of research in remote sensing. However, to acquire data with greater spectral and spatial coverage, a new instrument called the airborne visible-infrared imaging spectrometer (AVIRIS) is being developed (*15*). Using line arrays of silicon and InSb configured as in Fig. 2c, AVIRIS will acquire images in 224 bands 10 nm wide, in the 0.4- to 2.4-μm region. The instrument will fly in the NASA U-2 aircraft, and at an altitude of 20 km the swath width will be 11 km with a 20-m ground IFOV. In 1985 NASA will entertain proposals for analysis of AVIRIS data, and the instrument is scheduled for flight in 1986. A shuttle experiment also has been proposed and is scheduled for a 1986 funding start (*16*). A high-resolution imaging spectrometer is one of the Earth Observing System (EOS) instruments being considered for the Space Platform as part of the Space Station. EOS is slated for launch in the early- to mid-1990's (*17*).

Mineral Identification

In order to test the capability of imaging spectrometry for mineral identification with the AIS, the Cuprite mining district of Nevada was chosen for study. The Cuprite area contains both hydrothermally altered and unaltered rocks, well exposed and nearly devoid of vegetation. The altered rocks overflown in this study contain secondary quartz, opal, and clay minerals (*18*), and the area has been subjected to extensive study with broadband multispectral images in the visible, reflective, and emissive infrared (*19*). Several minerals, whose reflectance spectra were shown in Fig. 1, occur in the Cuprite area and have diagnostic absorption features in the 2.0- to 2.4-μm region. The narrow spectral band sampling possible with an imaging spectrometer should therefore allow these minerals to be identified.

Figure 4a shows the central region of the Cuprite district overflown with AIS. The bright areas are the result of trenching operations that break through the dark-stained surface crust and expose materials consisting of almost pure silica. The bottom curve in Fig. 4b shows a raw 128-channel spectrum of a 5 by 5 pixel area in the AIS coverage outlined in Fig. 4a. The major features are the broad atmospheric water bands centered at 1.4 and 1.9 μm and the solar irradiance curve, which exhibits a rapid falloff toward longer wavelengths. A shortcut to modeling the atmospheric and insolation effects can be made if one normalizes the data to an area in the image having little or no topographic relief and uniform, known spectral reflectance characteristics. The top curve in Fig. 4b is the result of this normalization procedure. Spectral features in the surface material become more apparent in the normalized spectrum because the removal of systematic effects makes it possible to display the data at their full radiometric resolution. Enhanced 32-channel images covering the region from 2.03 to 2.32 μm, and acquired in the area outlined in Fig. 4a, are shown in Fig. 4c. Surface features having absorption bands can be recognized by changes in contrast with respect to their surroundings.

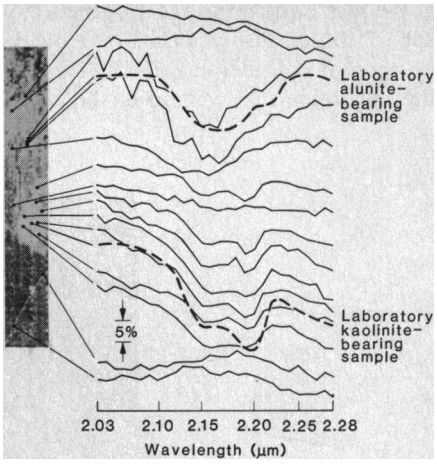

Fig. 5. AIS image from Cuprite, Nevada, showing 3 by 3 pixel spectra of three representative surface units. Direct identification of the dominant mineral in each area can be made on the basis of the 2.0- to 2.3-μm spectral response. Laboratory spectra of field-collected samples are also shown (broken lines), and they verify the AIS results.

Spectra can be derived on a pixel by pixel basis from any point on the AIS image. Figure 5 shows a single 9.3-nm-wide channel image at 2.03 μm taken from Fig. 4c and the reflectance spectra derived from averages of 3 by 3 pixel areas from all 32 images. Three general spectral classes are seen. The spectra taken from the hill in the lower portion of the image contain an absorption doublet which matches that of kaolinite [$Al_2(Si_2O_5)(OH)_4$]. A laboratory spectrum of a field sample from a spectral reference library is also shown. The spectra show a single, broad-absorption feature centered at 2.17 μm indicative of alunite [$KA1_3(SO_4)(OH)_6$], a mineral associated with altered feldspathic rocks. A laboratory reflectance spectrum of a field sample is superimposed. The spectra obtained from the top of the image are devoid of absorption features since this surface material consists of almost pure quartz, which does not exhibit spectral absorption features in this wavelength region.

Vegetation Mapping

Approximately 70 percent of the land surface of the earth is covered with vegetation. Native vegetation can be an accurate indicator of local and regional geologic conditions. In addition, vegetation is an indicator of stress agents of nongeologic origin. Nutrient deficiency response and insect damage are well characterized for some forest species (*20*), whereas anthropogenic and water-induced stresses produce varying types of response in susceptible species of both native and crop vegetation (*21*). Subtle features of the native vegetation such as variations in species and community distribution patterns, alterations in phenologic cycles, and modifications in the physiology and morphology of individual specimens provide valuable insight into the climatic, edaphic, geologic, and physiographic characteristics of an area. The use of vegetation conditions, health, chemical composition, and structure as a means of inferring geologic information constitutes an interdisciplinary approach known as geobotany.

Reflectance spectra of vegetation, gathered in the 0.4- to 2.5-μm region of the electromagnetic spectrum, contain information on plant pigment concentrations, leaf cellular structure, and leaf moisture content (*22*). Such botanically significant information, when gathered in the appropriate format, allows the remote discrimination and mapping of plant species or communities, the detection of their physiological condition and state of health, and the assessment of the amount of cover or biomass, based on unique spectral properties of a vegetated surface. High-spectral-resolution data sets in image format, such as those provided by AIS, demonstrate the potential application of such data for botanical and geobotanical purposes.

As part of a study of the value of high-spectral-resolution imaging in vegetation studies, AIS overflights of the Pico Anticline, near Piru, California, were conducted in December 1982 at a time when several types of native vegetation were senescent and dry. Other types of vegetation, notably evergreen broadleaf and conifer species associated with both the

live oak communities and the riparian woodlands, as well as irrigated areas, were photosynthetically active at the time of these overflights. The AIS data were acquired in the 1.2- to 1.5-μm region only, with a ground IFOV of approximately 10 m. Simultaneously, the NASA NS-001 thematic mapper simulator (TMS) acquired multispectral data in six broadband spectral regions, equivalent to the bands of the TM on Landsats 4 and 5. False-color infrared (CIR) aerial photography was also acquired.

Figure 6 shows a series of false-color images consisting of a CIR photograph, a principal components (PC) transformation (*23*) of TMS data for the same area, a similar PC of AIS data, and a duplicate AIS PC image with an overlay showing the areal distribution of dominant vegetation for the area. The TMS and AIS data, both of which have roughly equivalent radiometric resolution, were processed in an identical fashion in order to make possible a comparison of their respective capabilities.

The AIS PC image has more hues than the TMS PC image. Since the number of hues cannot be increased by simple contrast stretching, it can be assumed that more spectral variability is seen in the AIS data. This variability relates to the distribution of dominant species within the community. The results of the field-study identification are shown in the overlay. As an example, comparison of the AIS and TMS images shows that arroyo willow, mule fat, and bamboo are separable on the AIS image but not on the TMS.

These initial results demonstrate that the high-spectral-resolution, limited-spectral-coverage (1.2 to 1.5 μm) AIS image provides more species discrimination than the low-spectral-resolution, broad-spectral-coverage (0.4 to 2.5 μm) TMS image. The spectral region covered by the AIS contains reflectance features related to leaf structure and moisture content, characteristics likely to be related to species-specific conditions of senescence and physiology. More information, specifically concerning stress, will become available when the most important region, 0.5 to 1.2 μm, is covered with high-resolution imaging by AVIRIS.

Geobotanical exploration and environmental monitoring studies, based on the use of remotely sensed data acquired by high-spectral-resolution sensor systems such as AIS and AVIRIS, have the potential to provide information of physiologic and taxonomic significance to plant researchers. Such data, acquired essentially simultaneously for large areas of the earth and in a nondestructive fashion, will prove invaluable in developing capabilities for vegetation mapping, health assessment, and stress detection and characteristics.

Data Analysis

Just as imaging spectrometry requires new technology for instruments and detectors, effective utilization of the data requires development of new analytic approaches and techniques. Bellman's "curse of dimensionality" (*24*) is fulfilled with the advent of instruments that produce images in hundreds of spectral bands simultaneously. Bellman's comment arose in the context of multivariate statistical analysis, the dominant approach in today's methods of multispectral scene classification. Dimensionality is used here in the statistical sense and refers to the number of spectral measurements (variates) per pixel. The dimensionality of imaging spectrometer data makes it necessary to seek new analytic methods if dependence on the raw computational power of supercomputers is to be avoided. The experience with AIS

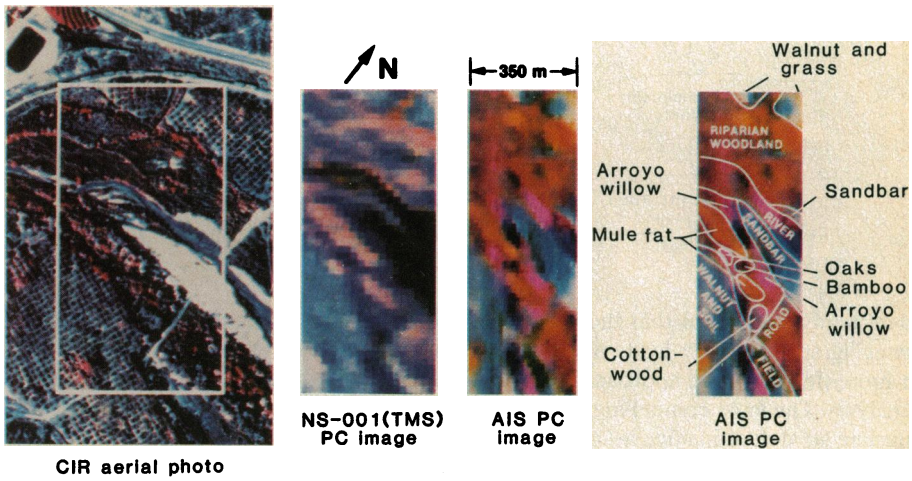

Fig. 6. Comparison of color infrared (CIR) aerial photography, principal components (PC), thematic mapper simulator (TMS), and AIS data acquired simultaneously over an area of orchards and riparian woodlands near Piru, California. A PC transformation was applied to the seven spectral channels of the TMS data and 18 of the 32 channels of AIS data in the 1.2- to 1.5-μm region exclusive of the 1.4-μm atmospheric water band. Equivalent contrast stretches were applied to each image. The results of ground species identification are shown on the right.

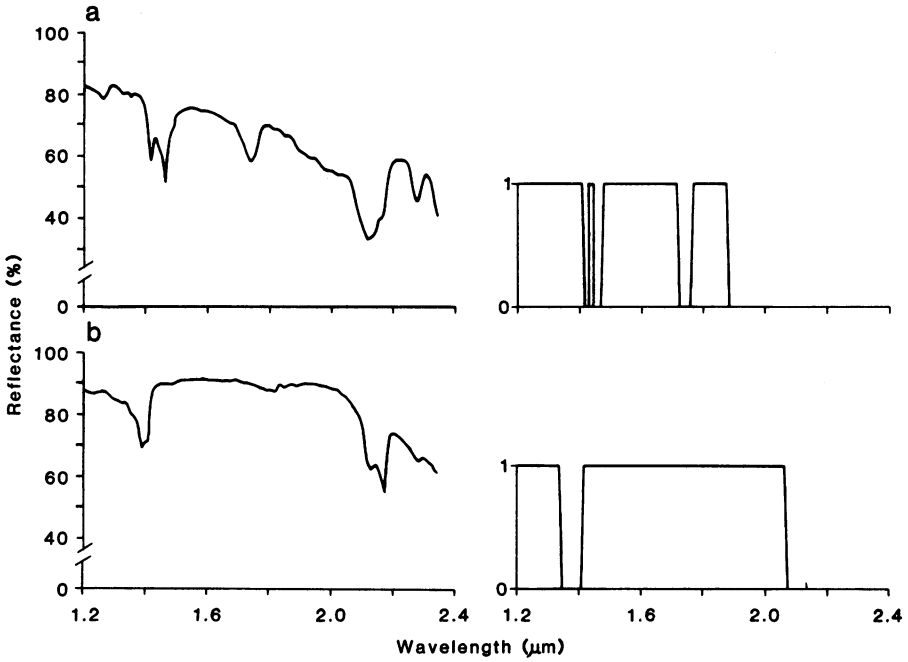

Fig. 7. Binary encoding scheme for laboratory reflectance spectra of two minerals, (a) alunite and (b) kaolinite.

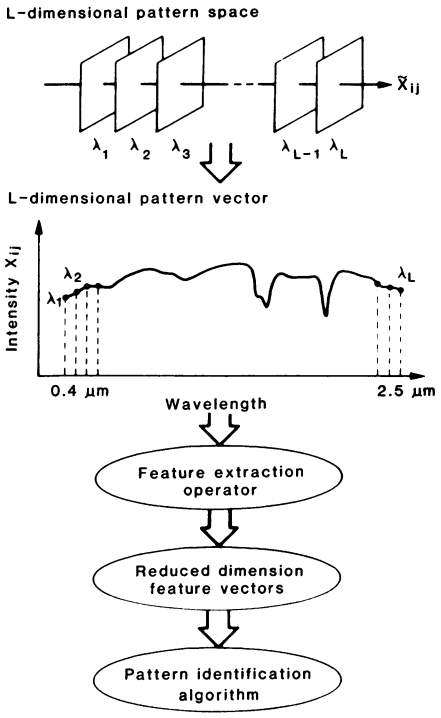

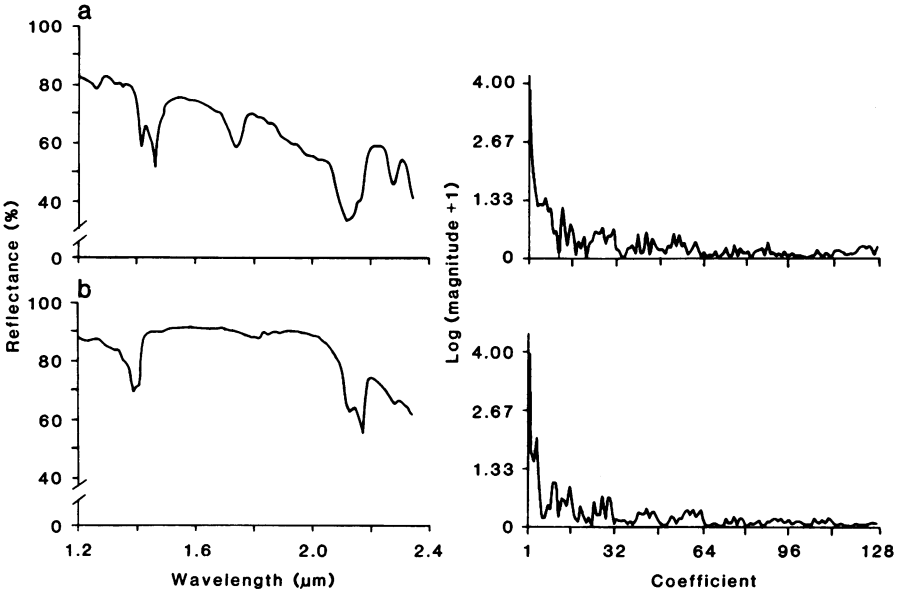

Fig. 8 (left). Generalized approach to the multispectral classification problem. Fig. 9 (right). Spectral reflectance curves of two minerals, (a) alunite and (b) kaolinite, and their corresponding Walsh-Hadamard spectral transformations. The value of the magnitude of the coefficients was increased by 1 to facilitate plotting of the magnitudes on a logarithmic scale.

data tends to confirm that the nature of imaging spectrometry leads naturally to a more deterministic approach to scene analysis. The most compelling reason for turning to deterministic, as opposed to statistical, methods of analysis is the fact that imaging spectrometry provides spectral sampling sufficient to define unique spectral signatures.

The first problem to be addressed in the analysis of these data is visual interaction with hyperspectral images and their statistical properties. Current graphics and image display technology allow implementation of a variety of tools for visual exploratory analysis. Among these are the ability to display a time-sequenced projection of the images in the spectral direction, cursor-designated spectral plots of single pixels or averages over a spatial window, and rapid location of pixels having similar spectral signatures. In addition, it is now possible to interactively locate and display spectra from a spectral library for visual comparison and to interactively create spectral data sets from specified regions in the scene. Figure 5 illustrates some of these capabilities based on the use of AIS data acquired over Cuprite, Nevada.

Another useful visual enhancement of the data is the application of an equal energy spectral normalization, given by

$$\sum_{\ell=1}^{L} A_{ij} X_{ij}(\ell) \text{ is constant} \qquad (1)$$

where ℓ is the wavelength index, (i,j) is the spatial location index, A_{ij} is the scalar multiplier for the intensity X_{ij} of pixel (i,j), and L is the total number of spectral measurements per pixel. The resulting normalized data allow direct comparisons of the shapes of spectral curves. An example of this enhancement is shown in Fig. 4c where the kaolinite doublet feature at location a becomes obvious.

Manual examination of the spectral content of the images by cursor-designated plotting is a useful tool. It becomes rather laborious, however, when one is trying to locate spectrally similar units throughout an entire scene. To overcome this problem, a fast spectral signature–matching algorithm has been devised that can be used to find all the pixels in a scene having a spectral signature similar to a specified prototype spectrum. The prototype can be specified from the image data itself or from a spectral reference library. The technique relies on binary encoding of the spectral data in order to achieve fast cross-correlation for signature matching. A number of approaches may be used in achieving the binary encoding. However, the following algorithm appears to give the best overall results. Using the same notation as in Eq. 1, we find that each pixel is written as an L-component vector

$$\vec{X}_{ij} = [X_{ij}(\lambda_1), X_{ij}(\lambda_2), \ldots, X_{ij}(\lambda_L)]^T \qquad (2)$$

where λ denotes wavelength and T denotes transpose. If we define the scalar, μ_{ij}, as the mean of the (i,j) spectral vector,

$$\mu_{ij} = \frac{1}{L} \sum_{\ell=1}^{L} X_{ij}(\ell) \qquad (3)$$

a binary-valued L-element vector, $\vec{Y}_{ij}$, is constructed by

$$\vec{Y}_{ij} = H(\vec{X}_{ij} - \mu_{ij}) \qquad (4)$$

where $H(u)$ is the unit step operator

$$H(u) = \begin{cases} 1, & u \geq 0 \\ 0, & u < 0 \end{cases} \qquad (5)$$

An example of the use of this encoding scheme is illustrated in Fig. 7, where the results are shown for laboratory reflectance spectra of two mineral samples.

In order to characterize the similarity between two binary spectral vectors, the Hamming distance (*25*) is used,

$$D_H(\vec{Y}_{ij}, \vec{Y}_{mn}) = L - \vec{Y}_{ij}\vec{Y}_{mn}^T \qquad (6)$$

or

$$D_H(\vec{Y}_{ij}, \vec{Y}_{mn}) = \sum_{\ell=1}^{L} Y_{ij}(\ell) \oplus Y_{mn}(\ell) \qquad (7)$$

where $\oplus$ denotes the logical exclusive OR operator (*26*). This distance measure is related to the more familiar Tanimato measure (*25*) used in taxonomic classification. In order to accommodate natural variability in spectra of similar materials, the algorithm is run with the use of a specific threshold of acceptance $D_H = \bar{d}$, such that

$$\vec{Y}_{ij} \doteq \vec{Y}_{mn} \text{ if and only if } D_H \leq \bar{d} \qquad (8)$$

This algorithm provides a fast means of searching a scene for the location of specific classes and has been used with success on AIS data (*27*).

Multispectral scene classification is especially affected by the dimensionality of imaging spectrometer data. The general multispectral classification problem is

illustrated diagramatically in Fig. 8. The key element in this problem appears to be finding a feature extraction operator with efficient information compression properties. The transformation operator can be linear or nonlinear but should reduce dimensionality and at the same time preserve the information necessary for identification of the spectral signature. One of the traditional transformations used is the Karhunen-Loeve, or PC, transformation (*23, 28*). However, construction of this transformation requires estimation of the covariance matrix, and this process would take on the order of 10^{13} arithmetic operations for a typical scene 10 by 10 km such as will be acquired by AVIRIS. Clearly, more computationally efficient transformations are needed for the analysis of imaging spectrometer data.

The nonlinear binary encoding and cross-correlation techniques discussed above are possible in this context. However, there is a large class of linear deterministic transformations having fast numerical implementations that are obvious candidates as feature extraction operators. Examples include Fourier, Walsh-Hadamard, and Haar (*28*). An example of the Walsh-Hadamard spectral transformation is shown in Fig. 9. All linear transforms provide dimensionality reduction. However, there remains the question of clustering properties and similarity measures in the reduced dimension pattern space. The Walsh-Hadamard transform (*28*) is particularly attractive from the standpoint of computational speed, being even faster than the fast Fourier transform. Furthermore, early analytic results indicate that a dimensionality reduction of eight to one can be achieved while good classification accuracy is retained.

Conclusion

Direct identification of Earth surface materials on the basis of their unique spectral reflectance features is now possible with imaging spectrometer systems in aircraft and eventually in spacecraft. New image-processing methods are being developed to handle the large quantities of data provided by these new sensors. Another step in machine analysis of data, the use of knowledge-based expert system methods for scene analysis (*29*), may eventually be required to make full use of the information content of these very large data sets. This approach offers great promise in providing an integrated data management and data analysis scheme suitable for handling data of the imaging spectrometer type. The ability of such systems to efficiently use a priori knowledge about spectral class characteristics, general scene content, and spatial association rules makes this approach quite attractive. Properly designed, such systems will provide for efficient user interactions and dynamic modification of both the knowledge base and its application to specific analytic problems.

References and Notes

1. A. F. H. Goetz and L. C. Rowan, *Science* **211**, 781 (1981).
2. J. F. McCauley *et al.*, *ibid.* **218**, 1004 (1982).
3. A. F. H. Goetz, L. C. Rowan, M. J. Kingston, *ibid.*, p. 1020; W. Collins, S. Chang, G. Raines, F. Carney, R. Ashley, *Econ. Geol.* **78**, 737 (1983); N. M. Milton, W. Collins, S. Chang, R. G. Schmidt, *ibid.*, p. 605.
4. S. C. Freden and F. Gordon, Jr., *Manual of Remote Sensing* (American Society of Photogrammetry, Falls Church, Va., 1983), chap. 12.
5. G. R. Hunt, *Geophysics* **42**, 501 (1977).
6. D. Meissner, H. Laucht, J. Bodechtel, R. Haydn, in *Proceedings of the 1983 International Geoscience and Remote Sensing Symposium* (IEEE Catalog No. 83CH1837-4, IEEE, New York, 1983), p. FA-4, 1.1.
7. G. Brachet, in *Proceedings of the 1981 International Geoscience and Remote Sensing Symposium* (IEEE Catalog No. 81CH8656-8, IEEE, New York, 1981), p. 1315.
8. G. DeClerck, J. Bosiers, J. Sevenhaus, L. Van den Hove, in *Proceedings of the IEEE International Electron Devices Meeting* (IEEE, New York, 1983), p. 505.
9. M. M. Blouke, J. R. Janesick, J. E. Hall, M. W. Cowens, P. J. May, *Opt. Eng.* **22**, 607 (1983).
10. J. R. Janesick and M. M. Blouke, in *Proceedings 28th Society of Photo-Optical Instrumentation Engineers Annual International Technical Symposium on Optics and Electro-Optics* (SPIE, Bellingham, Wash., 1984), vol. 501, p. 2.
11. G. C. Bailey, K. Matthews, C. A. Niblack, in *Proceedings of the Society of Photo-Optical Instrumentation Engineers* (SPIE, Bellingham, Wash., 1983), vol. 430, p. 52.
12. J. P. Rode, K. Vural, J. D. Blackwell, F. A. Cox, W. N. Lin, in *Proceedings of the Infrared Information Systems Specialty Group on Infrared Detectors* (IRIS, San Diego, 1982), p. 313.
13. J. B. Wellman, A. F. H. Goetz, M. Herring, G. Vane, in *Proceedings of the 1983 International Geoscience and Remote Sensing Symposium* (IEEE Catalog No. 83CH1837-4, IEEE, New York, 1983), p. FA-5, 6.1.
14. G. Vane, A. F. H. Goetz, J. B. Wellman, *IEEE Transactions on Geoscience and Remote Sensing* (IEEE, New York, in press).
15. G. Vane, M. Chrisp, H. Enmark, S. Macenka, J. Solomon, in *Proceedings of the 1984 IEEE International Geoscience and Remote Sensing Symposium* (Publication SP215, European Space Agency, Paris, 1984), p. 751.
16. J. B. Wellman *et al.*, in *Proceedings of the IEEE National Telesystems Conference* (IEEE Catalog No. 83CH1975-2, IEEE, New York, 1983), p. 286.
17. D. M. Butler *et al.*, *Earth Observing System* (Technical Memorandum 86129, National Aeronautics and Space Administration, Washington, D.C., 1984), vol. 1.
18. M. J. Abrams, R. P. Ashley, L. C. Rowan, A. F. H. Goetz, A. B. Kahle, *Geology* **5**, 736 (1977).
19. A. B. Kahle and A. F. H. Goetz, *Science* **222**, 24 (1983).
20. P. A. Murtha, *Can. For. Ser. Publ. 1292* (1972), p. 12.
21. B. N. Rock and J. E. Vogelmann, in *Proceedings of American Society of Photogrammetry* (American Society of Photogrammetry, Falls Church, Va., 1985), p. 860; P. A. Murtha, *Int. Arch. Photogramm.* **13(B8)**, 667 (1980); C. J. Tucker, *Remote Sensing Environ.* **10**, 22 (1980).
22. A. F. H. Goetz, B. N. Rock, L. C. Rowan, *Econ. Geol.* **78**, 573 (1983).
23. Principal components transformation is a linear transformation of multivariate data to a new coordinate system in which the axes are orthogonal and linear combinations of the original variates. The transformation is derived from the covariance matrix to produce a coordinate system in which the correlation among classes of materials based on spectral reflectance is minimized. The first three principal components were combined to produce the TM and AIS color images shown in Fig. 6.
24. R. O. Duda and P. E. Hart, *Pattern Classification and Scene Analysis* (Wiley, New York, 1973).
25. J. T. Tou and R. C. Gonzalez, *Pattern Recognition Principles* (Addison-Wesley, Reading, Mass., 1974), chap. 3.
26. J. C. Boyce, *Digital Logic and Switching Circuits* (Prentice-Hall, Englewood Cliffs, N.J., 1975).
27. J. E. Solomon and M. Lee, in preparation.
28. R. C. Gonzalez and P. Wintz, *Digital Image Processing* (Addison-Wesley, Reading, Mass., 1979).
29. R. O. Duda and E. H. Shortliffe, *Science* **220**, 261 (1983); M. Goldberg, G. Karam, M. Aluo, paper presented at the IEEE Computer Society Conference, Vision and Pattern Recognition, Washington, D.C., 1983; T. E. Weymouth, J. S. Griffith, A. R. Hansen, E. M. Riseman, in *Proceedings Fourteenth Defense Advanced Research Projects Agency Image Understanding Workshop* (DARPA, Washington, D.C., 1983), p. 168; L. N. Kanal, *IEEE Trans. Pattern Recognition Mach. Intell.* **PAMI-1**, 193 (1979).

30. The research described in this article was carried out at the Jet Propulsion Laboratory, California Institute of Technology, under contract with the National Aeronautics and Space Administration.

Imaging Spectrometry for Earth Remote Sensing

Alexander F.H. Goetz, Gregg Vane, Jerry E. Solomon and Barrett N. Rock

Science **228** (4704), 1147-1153.
DOI: 10.1126/science.228.4704.1147